博 士 論 文

# Facile Functionalization of Anodized Titanium Oxide with Carbon Nanohorns Enhancing Bone Formation

# （骨形成の促進を目的としたカーボンナノホーンによる陽極酸化チタンの表面修飾）

平成３０年３月申請

北海道大学

大学院歯学研究科口腔医学専攻

髙　田　紗　理

**Abstract**

Carbon nanohorn (CNH) is a rolled graphene like circular cone. Recently, we reported that CNHs can promote bone formation in the early stage of bone healing process. These results suggested that CNHs are promising for surface modification of dental implant materials which accelerate the osseointegration. In this study, the anodized titanium (AnTi) coated with CNHs (CNH/AnTi) was developed in order to accelerate osseointegration and AnTi covered with CNHs was obtained without undesired formation of large aggregates by using the electrodeposition technique with applied potential at 300V for 180 s. CNH/AnTi improved the osteoblast-like cell proliferation, while it did not have an effect on the differentiation for osteoblast-like cell. 7 days after implantation of CNH/AnTi in rat femur, more amount of bone formed on the surface compared to AnTi. In addition, certain parts of new bone tissue were contacted with CNHs directly. The implant coated with CNHs by electrodeposition demonstrated excellent biocompatibility with bone tissues and promoted osseointegration in early stage.

**Introduction**

Carbon nanomaterials such as carbon nanohorns (CNHs), nanotubes (CNTs), and graphene are promising nanomaterials for bone tissue engineering applications because

of their unique characteristics [1–10], namely superior cytocompatibility, mechanical strength and outstanding electrical properties [11,12]. In this regard, our group has reported the CNT-coated substrates that can lead to excellent adhesion and differentiation of osteoblasts based on a favorable biocompatibility of CNT-coated collagen sponges with bone [13–16].

Among the carbon nanomaterials, CNHs have sparked an interest in the biomaterial and biomedical fields [17,18] due to their excellent characteristics, such as low toxicity and huge inner nanospaces for drug loading.[19,20] Utilizing these characteristics, recently, we found that CNHs can promote bone formation in the early term; within 2 weeks [17]. When macrophages engulfed CNHs, they accelerated the differentiation of mesenchymal stem cells into the osteoblasts [21].

In bone tissue engineering, prompt osseointegration, which is a direct structural and functional connection between living bone and biomaterials [22], is highly desirable for implants. Dental implants are known as highly successful therapeutic options with predictable and long-term success rates. [23] The clinical success of dental implants indeed depends on the achievement of osseointegration [24]. Titanium (Ti) is the most commonly used biomaterial for dental implants because of its excellent mechanical and biological properties [25]. Surface modifications are known as useful approaches to enhance functionalities of Ti. Anodizing is employed to increase the surface roughness of the Ti layer by formation a Ti oxide ($TiO_2$) layer, improving wettability and biocompatibility of the Ti surface. Following chemical or physical functionalizations are often applied for further modifications to improve biocompatibility or to induce biological responses, such

as osteoblasts attachment, proliferation, and bone response[26,27]. Among the surface modification methods of Ti, electrophoretic deposition is a quite simple, convenient and powerful method [28]. However, it has not been reported the application for biomaterials by electrophoretic deposition using carbon nanomaterials including CNHs.

In this study, we elucidate the possibilities of CNHs functionalizing for anodized-Ti (AnTi) surfaces for bone formation. CNHs-functionalized AnTi was successfully prepared by a simple electrophoretic deposition method using the same apparatus to anodize Ti. The functionalized AnTi demonstrated excellent osteocompatibility compared to AnTi with significance in early stage. This method is beneficial for bone tissue engineering to prepare functionalized Ti biomaterials without any interventions, such as heating, etching or chemical treatments.

## Materials and methods

### *1. Specimen preparation*

#### *1.1. Anodizing Ti*

Ti plates (99.5 % Nilaco, Japan) were cut into disks 9.0 mm in diameter, and Ti wire (99.5 % Nilaco, Japan 1.0mm diameter) was cut into 5.0 mm lengths. The specimens were grinded incrementally with #600 to #1500 grit silicon carbide waterproof abrasive paper, and then washed with ethanol and distilled water in an ultrasonic cleaner for 5 minutes. Ti disc was connected with Ti wire by laser welding. Then they were shielded with a silicone clear nail manicure (Dear Laura, Japan) to leave only the disc part exposed. The prepared Ti disc or wire were connected to an anode and a Pt mesh (thickness:0.1 mm) was connected to a cathode. An aqueous solution of 0.025 M DL-α-glycerophosphate

disodium salt (DL-α-GP, >85 %, Tokyo Chemical Industry, Japan) and 0.2 M calcium acetate (99 %, Kanto Chemical, Japan) was used as the electrolyte for anodizing. The anodizing was carried out in a constant current mode upon reaching the preset voltage using a DC power supply (PMC500-0.1A, Kikusui, Japan). The current density was 30 $mA/cm^2$, and the anodic voltage used was 320 V. During anodic oxidation, the electrolyte was maintained at room temperature (25 °C). Upon reaching 320 V, constant voltage was maintained for 1 min.

*1.2 Electrodeposition of CNHs on anodized Ti*

CNHs were produced by $CO_2$ laser ablation of graphite without the metal catalysts [19]. CNHs were oxidized by air with increasing the temperature at 1 °C min−1 from room temperature to 500 °C, followed by cooling [29]. The CNH dispersed in 99.9% ethanol at 250 μg/mL. 3mL of the CNH dispersion was injected into 1cm cuvette. AnTi (Figure 1a) connected to an anode and Ti (Figure 1b) connected to a cathode. Both electrodes were inserted into a cuvette with keeping at a distance of 8.0 mm as shown in Figure 1c. DC voltages of 250, 300, 350 and 400 V were applied for 60, 120, 180, 240 s between these two electrodes using a power supply (PMC500-0.1A, Kikusui, Japan). The surface structure was observed by a scanning electron microscopy (SEM: S-4000, Hitachi, Japan). The area of CNH deposition was measured by Image-Pro Premier 9.1 (Nippon Rober, Media Cybernetics). Typical thickness of the deposited films was estimated by cross-sectional analysis using FE-SEM (JEOL, JIB-4600F).

*2. Cell culture*

Human osteosarcoma cells (Saos2) were suspended in Dulbecco's modified Eagle's medium (DMEM; Sigma-Aldrich, USA) containing 10 % fetal bovine serum (FBS; Biowest, USA) and 1 % penicillin/streptomycin (Pen Strep; Thermo Fischer

ScientificGibco, USA) at 50 units/ml penicillin and 50 μg/ml streptmycin. Anodized Ti (AnTi) and AnTi deposited CNHs (CNH/AnTi) were placed in the wells of a 48-well plate and 500 μL of the cell suspension at $1.0 \times 10^4$ cells/mL was seeded on the scaffold in the wells and then incubated at 37◦C in a 5% $CO_2$ atmosphere for 7 days.

After cell culture, we observed the cells on the specimens by SEM. The samples were washed three times with PBS and fixed with 2.5 % glutaraldehyde. After dehydration through a graded series of water-ethanol, they were dried using the critical-point method and sputter-coated with palladium-platinum for SEM observation.

After cell culture, 300 μl of the cell suspension containing 0.2 % IGEPAL CA630 (Sigma-Aldrich, USA), was added to each sample. The samples were frozen, thawed and homogenized. The sample solution was added to 100 μl of 4 M NaCl 0.1 M phosphate buffer (pH 7.4) and then centrifuged for DNA analysis. Picogreen (Thermo Fischer Scientific,USA) was used to measure the DNA content by means of a fluorometer (Infinite F200 PRO, Tecan, Switzerland), with the excitation filter set at 356 nm and the emission filter at 458 nm. Alkaline phosphatase (ALP) activity was measured with LabAssay kit (Wako, Japan) as decribed previously [15]. ALP activity was normalized by DNA content. The DNA content and ALP activity were determined in four samples.

*3. Animal experiments*

Twenty-four male Wistar-strain rats aged 10 weeks (body weight 300-330 g) were used. The rats were anaesthetized with isoflurane inhalation solution (Pfizer Inc., USA). Bone holes were drilled in the left femurs of rats with a round dental bur 1.0mm in diameter. AnTi or CNH/AnTi wires were inserted in the bone marrow space in the femurs. Animal experiments were performed in accordance with the Guide for the Care and Use of Laboratory Animals, Hokkaido University (14-0090).

After 1 and 4 weeks after surgery, rats were anaesthetized and perfused with 5% glutaraldehyde diluted in 0.1M cacodylate buffer (pH 7.4) through the left cardiac ventricle. Femurs were removed with implants, and immersed in 10 % neutral buffered formaldehyde. The hard tissue was decalcified with ethylene diamine tetra acetic acid (EDTA). After decalcified, the implants were removed from bone marrow as gently as possible not to decay interface between tissue and specimens then the samples were embedded in paraffin. The paraffin sections were sagittally sectioned to about 5 μm in thickness. Specimens were stained with hematoxylin and eosin stain and observed with an optical microscope (AX-80, OLYMPUS, Japan). They were examined for tissue responses such as inflammation and osteogenesis around the implants.

After optical microscope observation, certain part of sample mounted on the slide glass were used for TEM samples. The mounting agent was removed by xylene. The capsule filled the Epon resin was loaded on the part. Afterwards, slide glass was removed from the polymerized block surface by heating. The ultrathin sections were obtained using an ultramicrotome (Leica, Germany) with a diamond knife (DiATOME). The ultrathin sections were examined by TEM (JEM1400 80 V, JEOL Ltd., Japan).

The bone contact ratio [30] (BCR) was calculated to evaluate osteocompatibility. Histomorphometric analysis was performed using NIH Image (National Institutes of Health, USA). Twenty areas containing the implant and surrounding bone were chosen at random for each section. The length of direct contact of bone with CNH/AnTi was measured on histological sections. BCR was calculated by using the following equation.

$$BCR = \frac{\text{Length of the implant-to-bone contact directly (L1)}}{\text{Length of new bone at implant surface (L1+L2)}} \times 100(\%)$$

Statistical analysis was carried out using the Kruskal Wallis H-test and Mann–Whitney

U-test with Bonferroni correction.

**Result**

1. TEM observation after electrodeposition of CNHs on anodized Ti

Ti plates were successfully oxidized by anodizing with a DC power supply (Figure 1). The SEM observation verified that the $TiO_2$ layer with micro pores was formed after the anodizing (Figure 1b). As shown in the photograph of AnTi (Figure 2a) and CNH/AnTi (Figure 2b), electrodeposition afforded effectively AnTi covered by CNHs.

At the electric current flew for 180 s with applied potential at 250 V, few CNHs deposited AnTi (Figure 3a). With applied potential at 300V, CNHs covered the AnTi surface homogeneously (Figure 3b). When the voltage was increased to 350 V (Figure 3c) and 400V (Figure 3d) respectively, the areas of CNHs covered on the AnTi surface were decreased (Figure 3e). With applied potential at 300V, the CNHs deposited on the AnTi surface increased as the time of the electric current increased from 60 (Figure 3f) s to 120 s (Figure 3g) reaching an optimal, evenly dispersed deposit of CNHs at 180 s (Figure 3b). At 240 s that CNHs were aggregated in clumps on the surface (Figure 3h). With applied potential at 300V, the areas of CNHs deposited on the AnTi surface is largest in the time course (Figure 3i). The FE-SEM images indicated that the thickness of CNHs deposited on the AnTi was 0.2-0.3 μm across the surface and the micro pore structure was maintained (Figure 4).

2. Cell Morphology

Figure 5 shows the proliferation of the osteoblast like cells on the AnTi (Figure 5a) and CNH/AnTi (Figure 5b) at 7 days. The cells on both samples adhered and spread. The filopodia of the cells stretch to the CNHs (Figure 5d). The DNA content and ALP activity

of the cells cultivated for 7 days on each sample are shown in Figure 5c. The DNA content in the cells attached to the CNH/AnTi was significantly higher than that on the AnTi ($p < 0.01$). There was no significant difference between the samples for ALP activity normalized by DNA content ($p > 0.1$).

3. Bone formation after implantation

Immature bone tissue (asterisk area in the images) was observed in the space between each specimen and existed bone tissue at 7 days after surgery as shown in Figure 6 a and b. However many osteoblasts with cubic shape were aligned on newly formed bone, some part of new bone seemed to directly attach to specimens. In particular, some of CNHs of CNH/AnTi observed on the newly formed bone were found to contact to bone matrix (Figure 6e). Some CNHs seemed to be released from specimens were engulfed by macrophages (white allow head). The BCR of CNH/AnTi was significantly higher ($p<0.05$) than that of AnTi at 7 days (Figure 7). At 28 days after surgery, more amounts of bone formed around both sample compared with at 7 days (Figure 8a,b). CNHs layer was observed on the bone (Figure 8c) contacted with bone directly as shown in the TEM observations (Figure 8c, d).

**Discussion**

It is notable that the different applied potential resulted in different surface morphology of the CNH/AnTi. The AnTi covered with CNHs without large aggregates was obtained by electrodeposition with applied potential at 300V for 180 s. It is worth to state that any additional thermal treatment was not needed to deposit the carbon nanomaterial, in contrast with the method reported by Sirivisoot et al. which investigated the multiwalled

carbon nanotubes grown from the anodized Ti by a chemical vapor deposition (CVD) process [31]. It is also remarkable that the present method in this study does not require large-scale apparatuses unlike the CVD process. Consequently, we succeeded in facile deposition of CNHs onto AnTi without any extra substances.

In order to investigate the advantages of CNH/AnTi in biocompatibility and osteoconductivity, the CNH/AnTi prepared with applied potential at 300V for 180 s was used for *in vitro* and *in vivo* study because the surface was completely covered with CNHs without large aggregates. The DNA content in the cells attached to the CNH/AnTi was significantly higher than that on the AnTi ($p < 0.01$). There was no significant difference between the samples for ALP activity normalized by DNA content ($p > 0.1$). Therefore, CNH-coating on Ti improved the proliferation, while it did not have effect on the differentiation of osteoblast-like cells. This result supports our previous report that CNHs did not increase the ALP activity of human mesenchymal stem cells without macrophages but did increase ALP activity in the presence of macrophages [21].

These results revealed that CNHs had compatibility with bone tissue. Mountziaris and Mikos reported that novel strategies that exploit inflammatory signals have the potential to induce greater regeneration than the systems that only deliver growth factors [32]. These results suggested that CNH/AnTi was more advantageous for early bone formation than AnTi and that the CNH improved the osteoconductivity of AnTi. We have reported that CNHs on the PTFE membrane promoted bone formation on the rat calvarial bone defect within a period of 2 weeks and a high amount of CNHs was localized inside the macrophages around the newly formed bone [17]. In this study, the fewer macrophages were observed around CNH/AnTi but CNHs deposited on the AnTi might be regulators for a variety of immune system reactions without triggering any cytotoxicity.

## Conclusion

AnTi could be coated with CNH efficiency by electrodeposition. CNH/AnTi had favorable biocompatibility with bone. Moreover, CNHs promoted bone formation in the early stage. Depositing CNHs on AnTi is advantageous as implants which accelerates osseointegration in the early stage after surgery.


## Acknowledgements

E.H. wishes thank the KAKENHI Grant in-Aid for Scientific Research C (ID No. 17K11733). A.Y wishes to thank the KAKENHI Grant in Aid for Scientific Research B (ID No. 16H05518). A part of this work was conducted at Hokkaido University, supported by "Nanotechnology Platform" Program of the Ministry of Education, Culture, Sports, Science and Technology (MEXT), Japan.


## References


1) Marangon I, Ménard-Moyon C, Silva AK a., Bianco A, Luciani N, Gazeau F. Synergic mechanisms of photothermal and photodynamic therapies mediated by photosensitizer/carbon nanotube complexes. Carbon 97:110–23, 2016.

2) Miyako E, Deguchi T, Nakajima Y, Yudasaka M, Hagihara Y, Horie M, et al. Photothermic regulation of gene expression triggered by laser-induced carbon nanohorns. Proc Natl Acad Sci USA 109:7523–8, 2012.

3) Miyako E, Kono K, Yuba E, Hosokawa C, Nagai H, Hagihara Y. Carbon nanotube-liposome supramolecular nanotrains for intelligent molecular-transport systems.

Nat Commun 3:1226, 2012.

4) Murakami T, Ajima K, Miyawaki J, Yudasaka M, Iijima S, Shiba K. Drug-loaded carbon nanohorns: adsorption and release of dexamethasone in vitro. Mol Pharm 1:399–405, 2004.

5) Wang J, Hu Z, Xu J, Zhao Y. Therapeutic applications of low-toxicity spherical nanocarbon materials. NPG Asia Mater 6:e84, 2014.

6) Yang K, Feng L, Shi X, Liu Z. Nano-graphene in biomedicine: theranostic applications. Chem Soc Rev 42:530–47, 2013.

7) Battigelli A, Ménard-Moyon C, Bianco A. Carbon nanomaterials as new tools for immunotherapeutic applications. J Mater Chem B 2:6144–56, 2014.

8) Bianco A, Cheng HM, Enoki T, Gogotsi Y, Hurt RH, Koratkar N, et al. All in the graphene family - A recommended nomenclature for two-dimensional carbon materials. Carbon 65:1–6, 2013.

9) Orecchioni M, Cabizza R, Bianco A, Delogu LG. Graphene as cancer theranostic tool: progress and future challenges. Theranostics 5:710–23, 2015.

10) Orecchioni M, Jasim DA, Pescatori M, Manetti R, Fozza C, Sgarrella F, et al. Molecular and Genomic Impact of Large and Small Lateral Dimension Graphene Oxide Sheets on Human Immune Cells from Healthy Donors. Adv Healthcare Mater 5:276–87, 2016.

11) Tran P a., Zhang L, Webster TJ. Carbon nanofibers and carbon nanotubes in regenerative medicine. Adv Drug Deliv Rev 61:1097–114, 2009.

12) Girase B, Shah JS, Misra RDK. Cellular mechanics of modulated osteoblasts functions in graphene oxide reinforced elastomers. Adv Eng Mater 14:101–11, 2012.

13) Hirata E, Akasaka T, Uo M, Takita H, Watari F, Yokoyama A. Carbon nanotube-

coating accelerated cell adhesion and proliferation on poly (L-lactide). Appl Surf Sci 262:24–7, 2012.

14) Hirata E, Uo M, Nodasaka Y, Takita H, Ushijima N, Akasaka T, et al. 3D collagen scaffolds coated with multiwalled carbon nanotubes: Initial cell attachment to internal surface. J Biomed Mater Res B Appl Biomater 93:544–50, 2010.

15) Hirata E, Uo M, Takita H, Akasaka T, Watari F, Yokoyama A. Development of a 3D collagen scaffold coated with multiwalled carbon nanotubes. J Biomed Mater Res B Appl Biomater 90 B:629–34, 2009.

16) Hirata E, Uo M, Takita H, Akasaka T, Watari F, Yokoyama A. Multiwalled carbon nanotube-coating of 3D collagen scaffolds for bone tissue engineering. Carbon 49:3284–91, 2011.

17) Kasai T, Matsumura S, Iizuka T, Shiba K, Kanamori T, Yudasaka M, et al. Carbon nanohorns accelerate bone regeneration in rat calvarial bone defect. Nanotechnology 22:65102, 2011.

18) Murakami T, Sawada H, Tamura G, Yudasaka M, Iijima S, Tsuchida K. Water-dispersed single-wall carbon nanohorns as drug carriers for local cancer chemotherapy. Nanomedicine 3:453–63, 2008.

19) Iijima S, Yudasaka M. Nano-aggregates of single-walled graphitic carbon nano-horns. Chem Phys Lett 309:165–70, 1999.

20) Miyawaki J, Yudasaka M, Azami T, Kubo Y, Iijima S. Toxicity of Single-Walled Carbon Nanohorns. ACS Nano 2:213–26, 2008.

21) Hirata E, Miyako E, Hanagata N, Ushijima N, Sakaguchi N, Russier J, et al. Carbon nanohorns allow acceleration of osteoblast differentiation via macrophage activation. Nanoscale 8:14514–22, 2016.

22) Branemark PI. Osseointegration and its experimental background. J Prosthet Dent 50:399–410, 1983.

23) Chappuis V, Buser R, Brägger U, Bornstein MM, Salvi GE, Buser D. Long-Term Outcomes of Dental Implants with a Titanium Plasma-Sprayed Surface: A 20-Year Prospective Case Series Study in Partially Edentulous Patients. Clin Implant Dent Relat Res 15:780‑90, 2013.

24) Srinivasan M, Meyer S, Mombelli A, Müller F. Dental implants in the elderly population: a systematic review and meta-analysis. Clin Oral Implants Res 28:920–30, 2017.

25) Van Noort R. Titanium: The implant material of today. Vol. 22, J Mater Sci. p. 3801–111987.

26) De Angelis E, Ravanetti F, Cacchioli A, Corradi A, Giordano C, Candiani G, et al. Attachment, proliferation and osteogenic response of osteoblast-like cells cultured on titanium treated by a novel multiphase anodic spark deposition process. J Biomed Mater Res B Appl Biomater 88:280–9, 2009.

27) Sul Y-T, Johansson CB, Jeong Y, Wennerberg A, Albrektsson T. Resonance frequency and removal torque analysis of implants with turned and anodized surface oxides. Clin Oral Implants Res 13:252–9, 2002.

28) Umeyama T, Tezuka N, Kawashima F, Seki S, Matano Y, Nakao Y, et al. Carbon nanotube wiring of donor-acceptor nanograins by self-assembly and efficient charge transport. Angew Chemie, Int Ed 50:4615–9, 2011.

29) Fan J, Yudasaka M, Kasuya D, Azami T, Yuge R, Imai H, et al. Micrometer-sized graphitic balls produced together with single-wall carbon nanohorns. J Phys Chem B 109:10756–9, 2005.

30) Ayukawa Y, Okamura A, Koyano K. Simvastatin promotes osteogenesis around titanium implants. Clin Oral Implants Res 15:346–50, 2004.

31) Sirivisoot S, Webster TJ. Multiwalled carbon nanotubes enhance electrochemical properties of titanium to determine in situ bone formation. Nanotechnology 19:295101, 2008.

32) Mountziaris PM, Mikos AG. Modulation of the Inflammatory Response for Enhanced Bone Tissue Regeneration. Tissue Eng Part B Rev 14:179–86, 2008.

**Figure Captions**

Figure 1

SEM images of Ti surface after polishing (a) and AnTi (b). Representation of electro deposition process (c).

Figure 2

Photographs of AnTi (a) and CNH/AnTi (b).

Figure 3

SEM images of the AnTi deposited CNHs at DC voltages of 250 V (a), 300 V (b), 350 V (C) and 400 V for 180 s. The graph shows each area of deposition respectively (e). AnTi deposited CNHs at DC voltages of 300 V for 60 s (e), 120 s (f) 180 s (b) and 240 V (h). The graph shows each area of deposition respectively (i).

Figure 4

Cross sectional observation of AnTi (a) and CNH/AnTi (b) and high magnification

corresponding to the white frame (c) by FE-SEM. An：Anodized titanium pore layer, O：Anodized titanium compact layer, Ti：Titanium layer, Au：Vapor deposition Au layer

Figure 5

SEM observation after 7days cell culture on the AnTi (a), CNH/AnTi (b) and the higher magnification (d). DNA content (left) and ALP/DNA activity (right) of the cells cultured on AnTi (grey) and CNH/AnTi (black) for 7 days (c) ; n = 5. The asterisk* indicates a statistically significant difference at $p < 0.01$.

Figure 6

The histological observation at 7 days after surgery: AnTi group (a) and at higher magnification (c), CNH/AnTi group (b) and high magnification (d) and high magnification corresponding to the white frame (e). Im: the area removed AnTi or CNH/AnTi., asterisk: newly formed bone;M.

Figure 7

Comparison of BCR at 7days. Asterisk indicate significant differences at $* p < 0.05$.

Figure 8

The histological observation at 28 days after surgery: AnTi group (a) and CNH/AnTi group (b). Im: the area removed AnTi or CNH/AnTi., asterisk: newly formed bone;M.
(c) TEM images of the part corresponding to the white flame in (b) and at high magnification corresponding to the white frame (d).

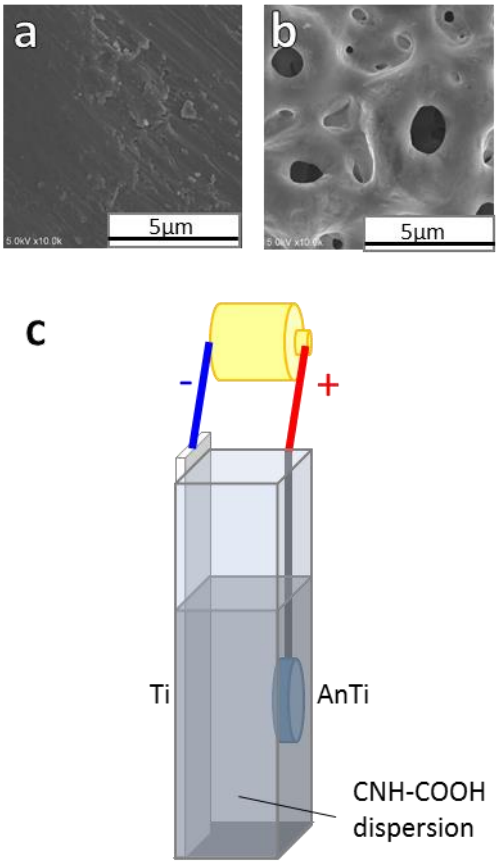


Figure 1

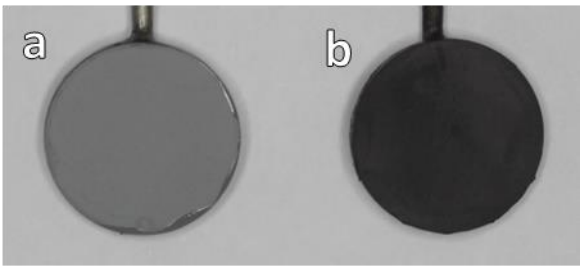


Figure 2

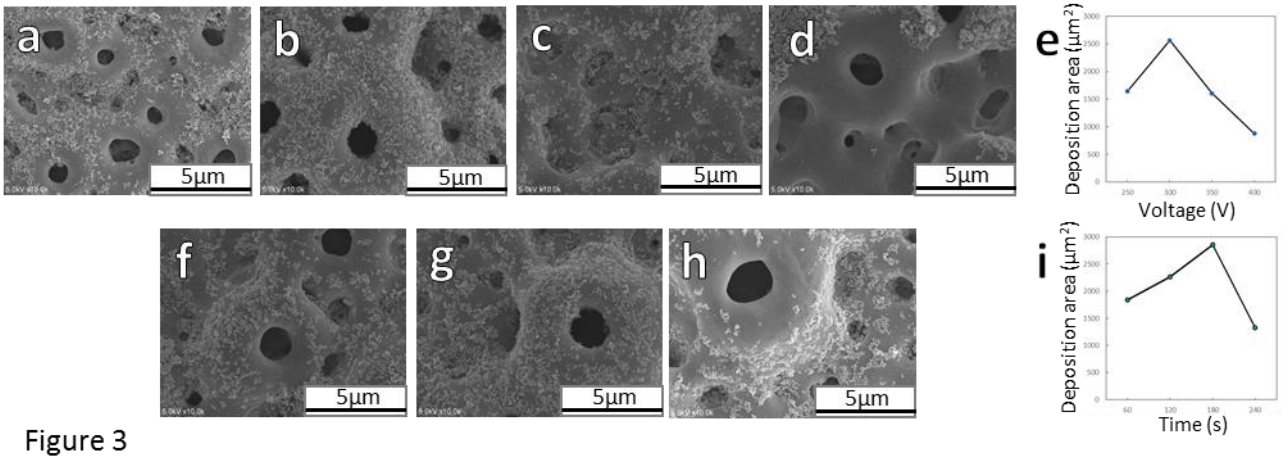


Figure 3

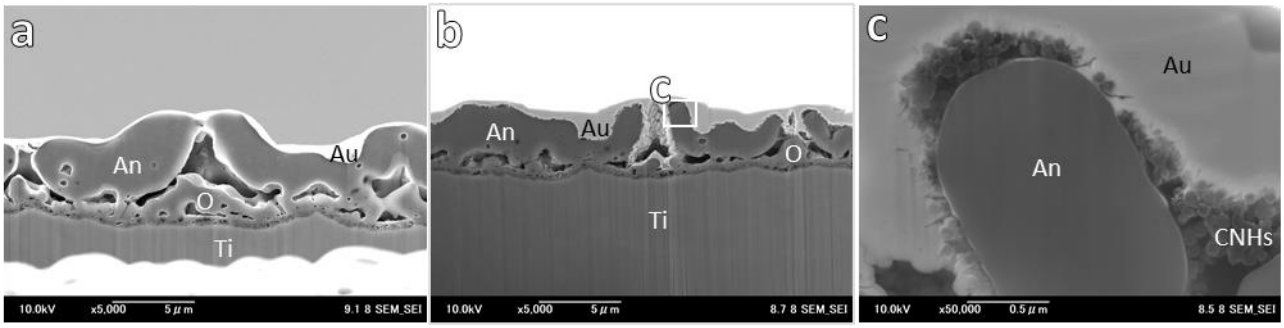


Figure 4

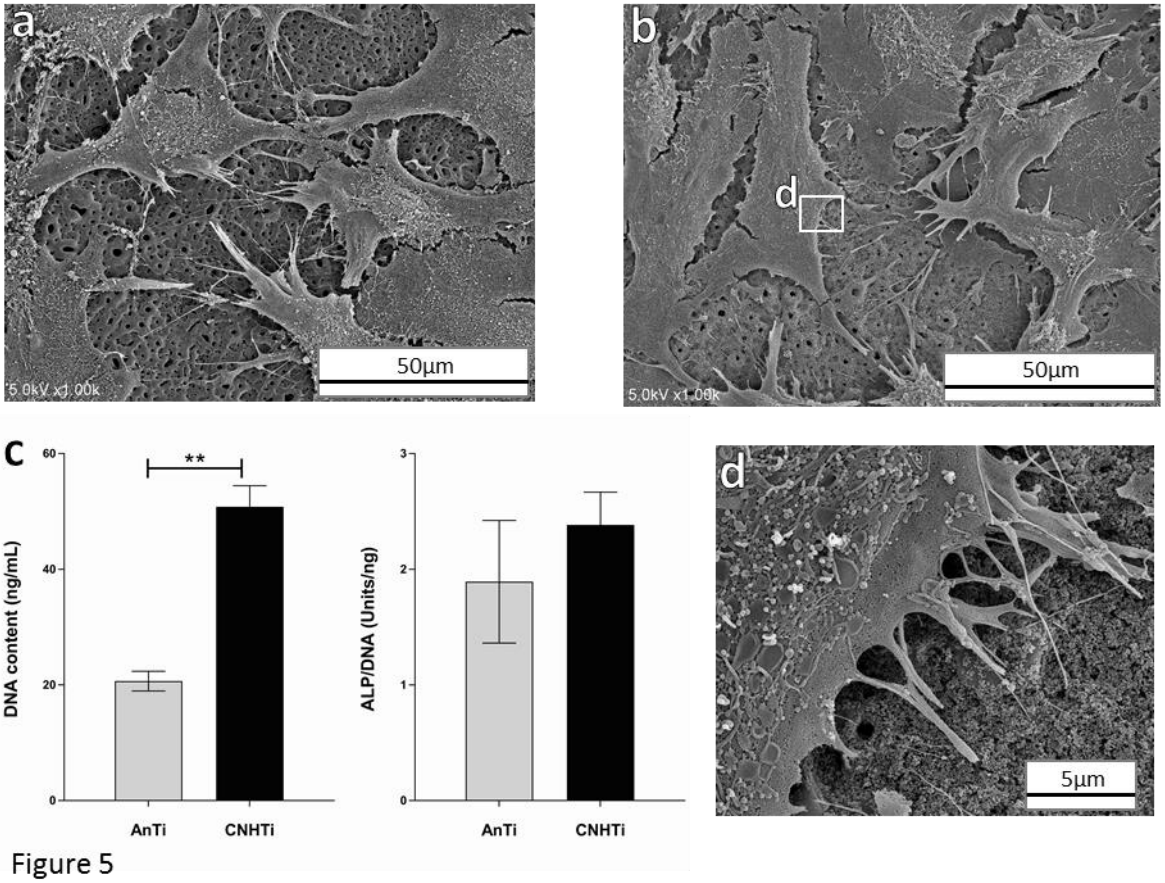
a
50µm
5.0kV x1.00k
b
d
50µm
5.0kV x1.00k
C
DNA content (ng/mL)
60
40
20
0
**
AnTi
CNHTi
ALP/DNA (Units/ng)
3
2
1
0
AnTi
CNHTi
d
5µm

Figure 5

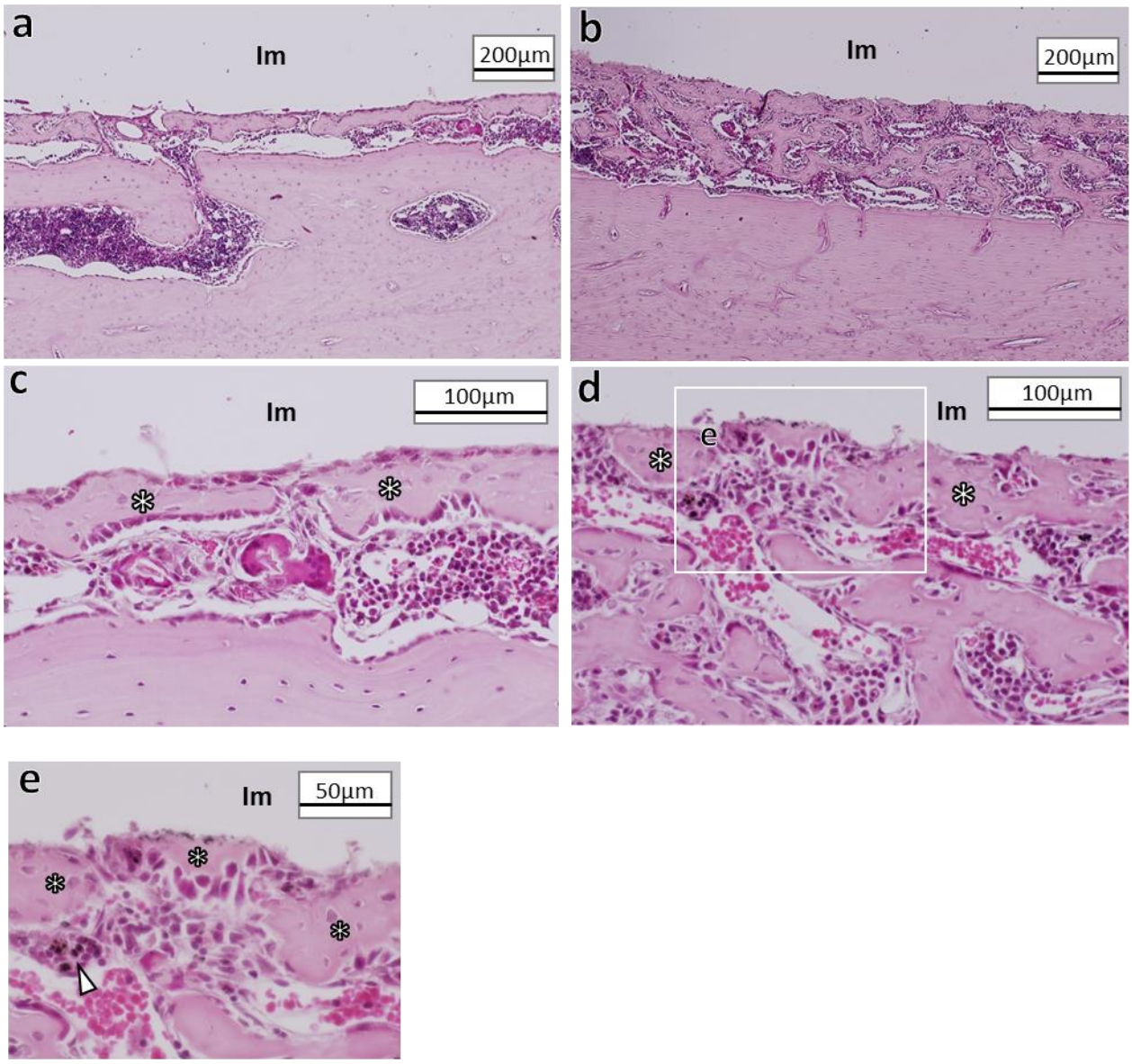


Figure 6

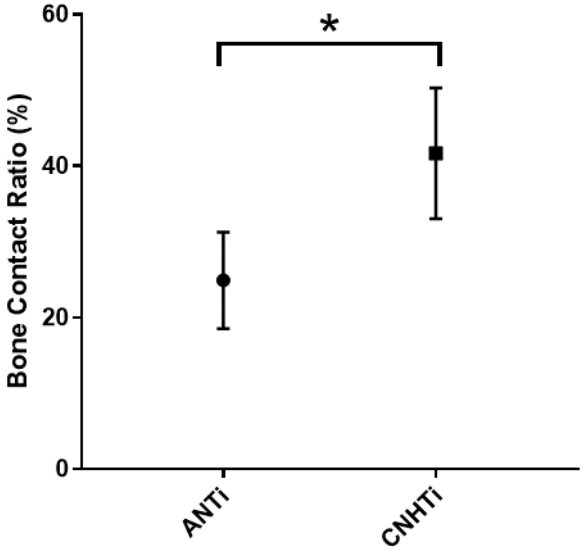


Figure 7

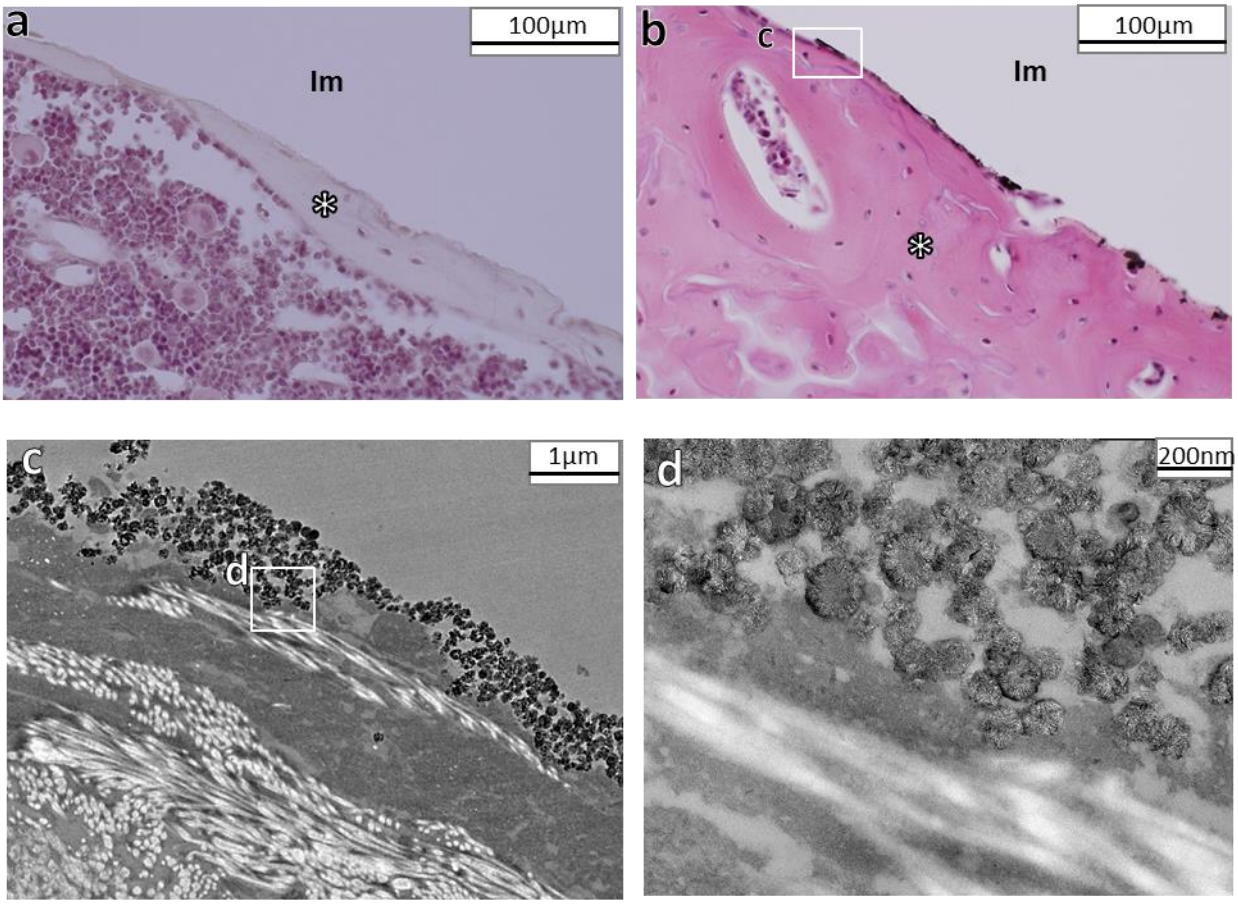


Figure 8